Wavefront shaping through a free-form scattering object

ALFREDO RATES,[1,*] AD LAGENDIJK,[1] AURÈLE J. L. ADAM,[2] WILBERT L. IJZERMAN,[3,4] AND WILLEM L. VOS[1]

[1]*Complex Photonic Systems (COPS), MESA+ Institute for Nanotechnology, University of Twente, P.O. Box 217, 7500AE Enschede, The Netherlands*

[2]*Optics Research Group, Department of Imaging Physics, Delft University of Technology, Lorentzweg 1, 2628 CJ Delft, The Netherlands*

[3]*CASA, Department of Mathematics and Computer Science, Eindhoven University of Technology, PO Box 513, 5600MB Eindhoven, The Netherlands*

[4]*Signify Research, High Tech Campus 7, 5656AE Eindhoven, The Netherlands*

[*]*a.ratessoriano@utwente.nl*

Abstract: Wavefront shaping is a technique to study and control light transport inside scattering media. Wavefront shaping is considered to be applicable to any complex material, yet in most previous studies, the only sample geometries that are studied are slabs or wave-guides. In this paper, we study how macroscopic changes in the sample shape affect light scattering using the wavefront shaping technique. Using a flexible scattering material, we optimize the intensity of light in a focusing spot using wavefront shaping and record the optimized pattern, comparing the enhancement for different curvatures and beam radii. We validate our hypothesis that wavefront shaping has a similar enhancement regardless of the free-form shape of the sample and thus offers relevant potential for industrial applications. We propose a new figure of merit to evaluate the performance of wavefront shaping for different shapes. Surprisingly, based on this figure of merit, we observe that for this particular sample, wavefront shaping has a slightly better performance for a free-form shape than for a slab shape.

1. Introduction

How to transport light efficiently from A to B? This deceivingly simple question is the central challenge in the functionality of daily used devices such as cameras, projectors, lighting systems, and even optically secured bank cards. When light travels from point A to B through a transparent medium with macroscopic, optionally curved, surfaces it follows a path that — following the famous principle of Fermat (1658) — has an optical length which is an extremum [1]. This changes fundamentally when the medium contains microscopic particles that scatter light. The technologically relevant question "what happens when both macroscopic curved interfaces and nanophotonic scattering media appear simultaneously", has remained unaddressed and unanswered yet. To date, free-form optics and nanophotonics have developed separately from each other, the former originating from optical engineering and the latter from condensed matter physics. The interplay between microscopic scattering and refraction or reflection by macroscopic free-form surfaces offers new, largely unexplored, opportunities and solutions to diverse technological problems.

The question of how light travels efficiently from A to B is central to many advanced technologies that play important roles in modern society, such as high-precision metrology for integrated nano-circuits in the Internet of Things (IoT) applications and our smartphones, or detectors in earth-observing satellites. In modern optics, the question is addressed by custom-designing free-form components – lenses and curved mirrors – that transfer a given distribution of light at the source to a desired distribution at the target in real space, or a sold angle in angle space. Over the last decade, free-form optics have been used in the development of versatile, miniature, and efficient devices that appear in daily life [1, 2].
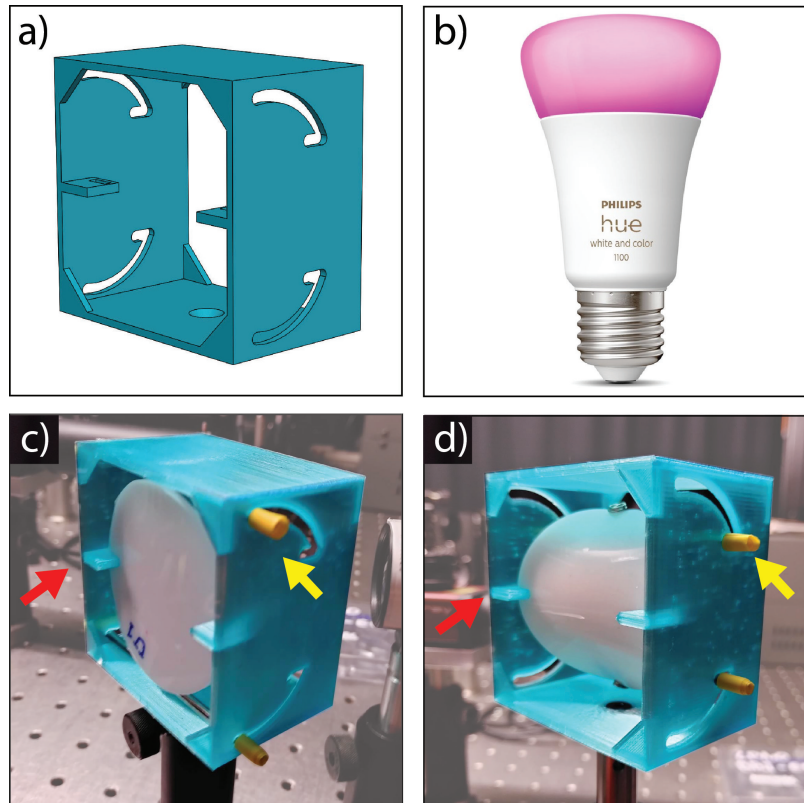
Fig. 1. Tailored-made holder and sample used for experiments. a) 3D model of the sample holder. b) Commercial smart light bulb, Philips HUE, from which the free-form shape of our sample is inspired. c) The sample in the sample holder in the flat position, and d) the sample in the curved position. The sample is attached horizontally to the holder (red arrow) and vertically to two movable metal bars (yellow arrow). The bars move in the range delimited by the rails on the side of the holder.

While nanophotonic media that scatter light cannot be understood with current free-form design methodologies, many modern devices greatly benefit from these media. For instance, in our homes, offices, and streets, a quiet revolution is taking place as white LEDs are replacing energy-inefficient light sources. A white LED consists of a blue diode [3], whose output is converted and diffused in a layer of phosphor particles [4, 5]. The presence of the light-scattering (and also absorbing and re-emitting) phosphor layer is essential to the functionality of a white LED. Other applications of nanophotonic media include high-precision metrology tools for nanolithography, the calibration of space instruments for earth observations, and novel (quantum) optically secured information technology for privacy. Currently, it is not feasible to describe light-scattering coatings, diffusers, or suspensions with free-form optics. Conversely, in nanophotonics, analytic solutions exist only for simple sample geometries such as a sphere, slab, and plane. No analytic solutions exist for arbitrary free forms. The presence of microscopically structured materials in macroscopic free forms implies a huge difference in scale to which conventional optical models cannot be applied. Hence current industry solutions invoke shortcuts, including untested assumptions (*e.g.* material homogeneity or disregard wavelength dependence). Today's lack of knowledge on free-shape scattering optics hampers fast, efficient, and systematic design progress as well as the development of new optical architectures.

One method extensively used for studying nanophotonic scattering media is wavefront shaping (WFS), where the light propagation through a scattering medium is controlled by interference [6–10]. These interferences generate a random pattern in the far field, called the speckle pattern. Recently, the potential of WFS has been extended to, for instance, time-varying samples [11–13], and periodic samples such as 2D (and 3D) photonic crystals [14, 15]. The interferences inside a scattering media are considered random. But still, when certain properties are slightly changed, a correlation in the speckle pattern persists. The phenomenon of persisting correlations is called the memory effect and has been studied by changing the angle of the incident beam, its position on the sample, and its wavelength [16–19]. But for all these experiments, the sample's shape was kept constant.

In most cases to date, WFS has been done on the quintessential scattering sample shape, namely in slabs. However, as previously illustrated, real-world applications require samples to have a free-form shape and be finite. Although many robustness studies have been made in WFS, as far as we know, no study includes changes in the sample's shape. Because of that, the impact of the macroscopic characteristics of the object is not addressed in current theories.

Here, we present the study of an opaque sample of TiO_2 particles suspended in silicone, as shown in Fig. 1. Exploiting the mechanical flexibility of silicone, we modify the shape of the sample and measure the enhancement of the intensity η in a portion of the speckle pattern in angle space, *i.e.*, a solid angle. We used a tailored-made sample holder to change both the curvature of the flexible sample and a focusing lens with a linear stage to change the beam radius on the sample. When it is curved, the sample has a curvature radius of approximately $R_c = 15$ mm. The thickness and the radius of curvature of the slab are inspired by the dimensions used in, *e.g.*, the Philips HUE bulb, see Fig. 1b). In this product, a set of colored LEDs is used to create both colored and white light at will using wireless control. To mix the light of these LEDs, the outer bulb plays an instrumental role. The typical thickness of the bulb is close to 2 mm, and the radius varies with position, of which we considered 15 mm a typical value. We compare the performance of WFS in a flat and a free-form sample as a function of beam radius. With this, we want to draw the attention of the community to study the properties of industrially relevant free-form scattering objects both in theory and experiments.

2.   Experimental Methods

The optical setup is depicted in Fig. 2. We use a green laser (Coherent COMPASS 315M-100, $\lambda = 532$ nm) as a source, and we modulate the wavefront using a digital micromirror device (DMD, DLP7000 Texas Instruments). To convert the binary amplitude modulation into a phase modulation, we use the Lee Holography technique [20, 21] implemented with a 4f system, where we filter the −1 order in the Fourier plane with an iris. The beam is then focused into the scattering material, placed in a tailored-made holder, and a CCD camera (Guppy PRO F-125b) collects the light transmitted through the sample. The focusing lens L5 is placed on top of a linear stage to have control over the position of the sample related to the focal length. The information collected from the CCD camera is used to optimize the DMD pattern following the sequential algorithm [6, 22].

The sample consists of TiO_2 particles suspended in silicone with a weight concentration of 0.1 wt%. The sample has a wafer-like shape with a thickness of $d = 2$ mm. To study the free-form sample, we exploit the flexibility of silicone to do measurements when the sample is flat and perpendicular to the incident beam and when the sample is curved. To curve the sample in a controlled manner, we designed a special sample holder, shown in Fig. 1. The sample is attached to the holder from the side with clamps and on the top and bottom to sliding metallic bars. These fixed points are highlighted in Fig. 1c) and Fig. 1d) with yellow and red arrows, respectively. When the bars are close to the front, the sample is completely flat, and when the bars are fixed close to the back, the sample is curved. With this holder, we control the curvature of the
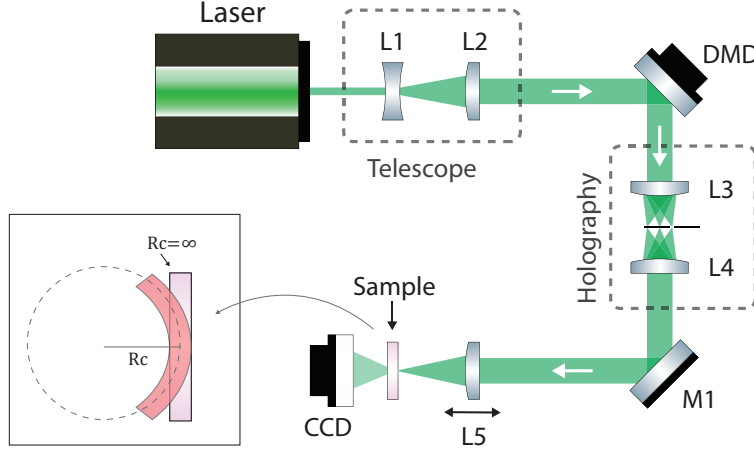
Fig. 2. Experimental setup for Wavefront Shaping. We use a DMD device combined with the Lee holography method to achieve phase-only modulation. Lens L5 is placed on top of a linear stage, to control the distance between L5 and the sample. We collect the speckle pattern in transmission. Inset: diagram of the curvature of the sample R_{c}. The sample is curved in such a way that the position of the center of the sample is constant. The sample is curved using the holder shown in Fig. 1. (L: lens; M: mirror).

sample during scattering and wavefront shaping experiments while other physical parameters are constant.

3. Enhancement in curved objects

A relevant parameter to study in WFS experiments is the intensity enhancement η. The enhancement is defined as

$$\eta \equiv \frac{I_{\mathrm{opt}}}{\langle I_0 \rangle}, \tag{1}$$

where I_{opt} is the intensity at a solid angle after wavefront optimization and $\langle I_0 \rangle$ is the ensemble average intensity of the pattern before optimization [23]. The ensemble average intensity is calculated by averaging the total counts on the detector at the target position over multiple random wavefronts. The enhancement increases when the number of segments N increases. A *segment* is a finite area of the incoming modulated wavefront that has the same phase value.

We compare a free-form sample with a slab-like shape by measuring the enhancement η for a different number of segments N_{s}. In Fig. 3, we plot $\eta(N_{\mathrm{s}})$ for both a flat and a curved sample. Each symbol is composed of the maximum enhancement obtained with the corresponding number of segments, averaged over three iterations of the optimization loop. Every iteration uses a flat incident wavefront as the initial value, meaning each optimization is independent of the others but starts from the same initial condition. Fig. 3 also includes two curves corresponding to theoretical limits. We see that the maximum theoretical limit is considerably above the experimental data. The discrepancy between the maximum limit and experimental data is because the limit does not take into account variations in the speckle size. In section 4 we will elaborate an extension of the theoretical limit, which yields values much closer to the experimental data.

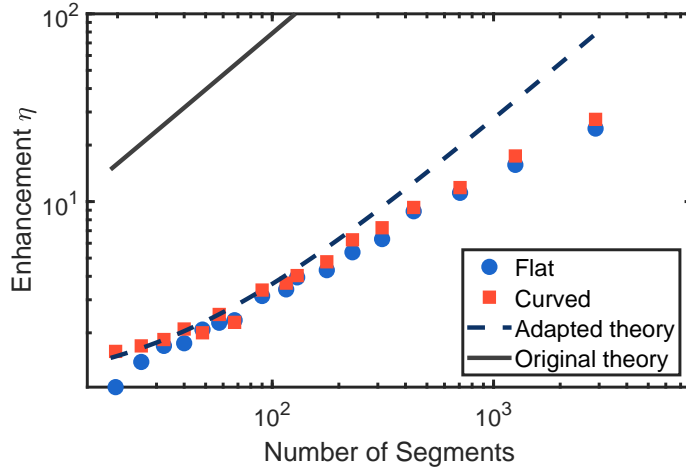Fig. 3 shows that both shapes give the same trend in enhancement, suggesting that the

Fig. 3. Enhancement versus the number of active modulating segments. The diameter of the illumination area is $2r_b = 4.5mm$. The blue circles represent the enhancement when the sample is flat and the red squares are for the curved sample. Each symbol is an average from three independent repetitions of the optimizations. The dashed line is the theoretical curve after correcting for the variable speckle size, while the solid line is the maximum theoretical curve without correction. Wavefront shaping is as effective in optimizing the intensity of a curved sample as it is with a flat sample.

performance of the wavefront shaping technique is the same regardless of the macroscopic properties of the object. This performance persistence is in agreement with our hypothesis and current theory of wavefront shaping [24, 25]. If we represent the scattering object as a random transmission matrix, regardless of the value of each coefficient, the efficiency of the wavefront optimization is unchanged. A possible effect that would cause a change in the total enhancement is if the number of open channels changes, changing the saturation point of the enhancement. Our data shows no sign of a change in saturation, meaning the number of open channels is seemingly unchanged.

An alternative interpretation of these results is that the curvature is simply not affecting the light transport inside the material or that it only affects the border of the optimized wavefront with a curvature effect. To test this new hypothesis, we calculate the correlation between the optimized wavefront of different measurements. For each number of segments, we have a total of 6 measurements, three from a curved sample and three from a flat sample. We take the optimized wavefront for each measurement, and we calculate the Pearson correlation coefficient between the 6 cases. We use the SciKit python library to calculate the correlation, which is defined as [26]

$$C_P \equiv \frac{\sum_{i,j}(x_{i,j} - \overline{x})(y_{i,j} - \overline{y})}{\sqrt{(\sum_{i,j}(x_{i,j} - \overline{x})^2(y_{i,j} - \overline{y})^2)}}, \tag{2}$$

with $x_{i,j}$ the value of segment (i, j) of the first wavefront, $y_{i,j}$ the value of segment (i, j) of the second wavefront, and $\overline{x}, \overline{y}$ the average segment values of the first and second wavefront, respectively.

We separate the correlations of wavefronts into three classes: the cross-correlations between wavefronts for a flat and a curved sample C_{cross}, the correlation between wavefronts with flat shape C_{flat}, and the correlation between wavefronts with curved shape C_{curve}. For the cases
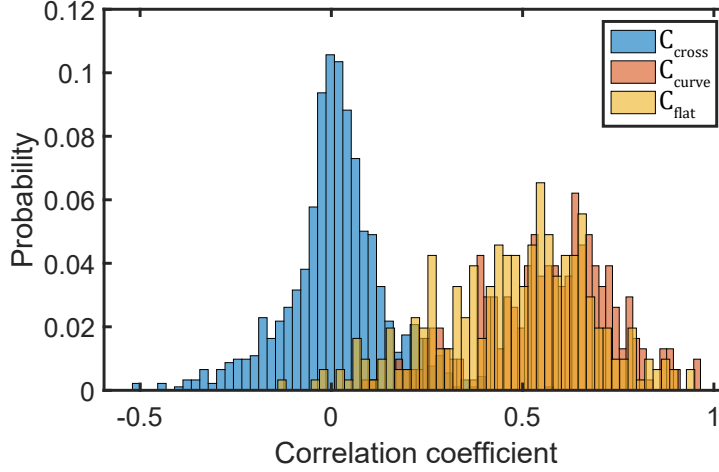
Fig. 4. Correlation distribution between optimized phase patterns. The blue distribution corresponds to the correlation between patterns from different shapes, while the orange and yellow distribution corresponds to the correlation between the same sample's shape (curve and flat, respectively).

where the sample's shape is not changed (C_{flat} and C_{curve}), we expect the optimized wavefronts to converge to a similar configuration, therefore, a high mutual correlation, regardless of the hypothesis we mentioned before.

If the macroscopic shape does affect the light transport when we change the sample's shape, we expect the optimized wavefront to converge to a new configuration, therefore C_{cross} to be small. On the other hand, if the macroscopic changes do not affect the light transport, then we expect the same value of C_{cross} regardless of the sample's shape.

The probability distribution of the correlations is shown in Fig, 4. We see that C_{cross} is centered at 0 and extends from about -0.3 to $+0.3$. In contrast, both C_{flat} and C_{curve} have higher and mostly positive correlations, between 0 and 1 and centered near 0.5. From this difference, we conclude that the macroscopic shape of the object affects the light transport inside it, and to control the scattered light in a free-form shape, we need a new optimized wavefront compared to the flat shape.

In the field of light scattering, the *memory effect* is a widely known property [16, 18, 25, 27]. The memory effect shows that when the light transport inside the scattering media is slightly changed, the speckle (and thus the optimized wavefront) are correlated with the previous one. As both speckle patterns are correlated, the same optimized wavefront can be used to enhance the intensity. From our observation that curved wavefronts are nearly uncorrelated with flat wavefronts, we conclude that the change in curvature is beyond the range of the memory effect. In previous studies, the light transport is changed by displacing the scattering media, tilting the incident beam, or changing the wavelength of the source. We thus believe our work is the first step towards studying the free-form memory effect, *i.e.*, the memory effect when changing the shape of the scattering media.

In theory, we expect the distributions of C_{flat} and C_{curve} to be centered at 1, while they are centered at 0.5. We attribute this to the fact that the DMD is not evenly illuminated because the laser beam has a Gaussian profile. Thus, the segments at the edges do not affect the optimization significantly and hence the $(x_{i,j}, y_{i,j})$ from Eq. 2 are different between one iteration and the other, thereby decreasing the correlation.
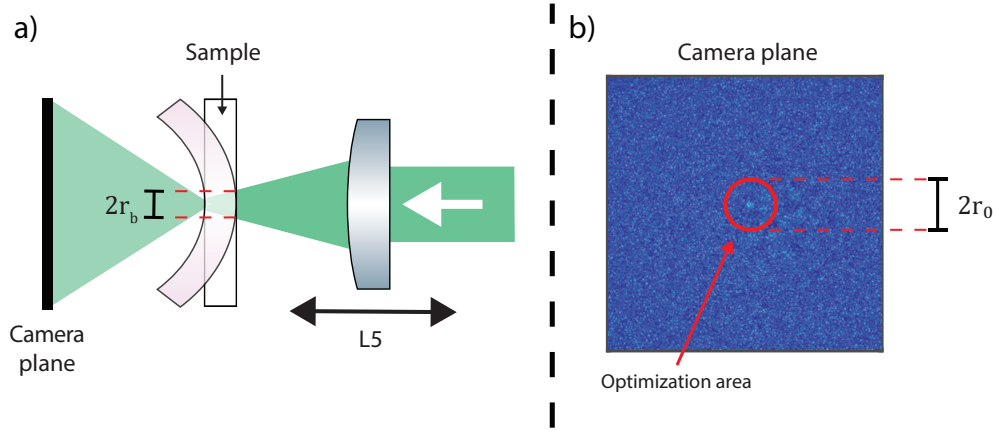
Fig. 5. a) Cartoon diagram of the illumination area, defined by its radius r_b. This depends on the distance between lens L5 and the sample. The curvature of the diagram is exaggerated for a didactic purpose. b) Diagram of the optimization area on the camera, defined by its radius r_o. This depends on the speckle size at the detector. To maintain a standard comparison, we keep r_o constant in our experiments.

From a geometrical-optics perspective, one might argue that even in the absence of scatterers, the curvature of the sample could sufficiently impact the wavefront to induce decorrelation of the optimized wavefronts. If this were indeed the case, one would anticipate that any decorrelation induced by the geometry would exhibit a pattern consistent with the curvature, *i.e.*, the central region of the wavefront being less affected than its edges. However, upon closer examination of each individual segment, we observe that the decorrelation is due to random changes in the complete wavefront, rather than following the expected curvature-related trend. Thus, we dismiss this possibility.

4. Enhancement in presence of variable speckle size

To estimate the maximum enhancement possible η_0 in WFS, one generally invokes wave-guide approximations typical of random matrix theory [24, 28–30] and simplify the scattering medium as a set of scattering channels. For this study, We will focus on the intensity enhancement of a single speckle spot as the figure of merit (other types of optimizations are, *e.g.*, enhance the total transmission of the system). The maximum enhancement η_0 is obtained when all the channels are optimized. η_0 expressed as

$$\eta_0 = \frac{\pi}{4}(N_s - 1) + 1, \tag{3}$$

where N_s is the total number of segments used in the modulator. This equation is valid for phase-only modulation and does not consider the saturation point when N_s is equal to the number of transmission channels inside the sample N_c.

To compare η_0 with our experiments, we need to distinguish between the beam radius r_b and the optimization radius r_o. This difference is illustrated in Fig. 5, where r_b is the radius of the illumination area at the sample surface that depends on the focusing lens L5 and the position of the sample. Conversely, r_o is the radius of the area of the speckle pattern that we observe at the detector, and it is relative to the speckle size of the speckle pattern. Because we have a lens-less system, this area represents a solid angle.
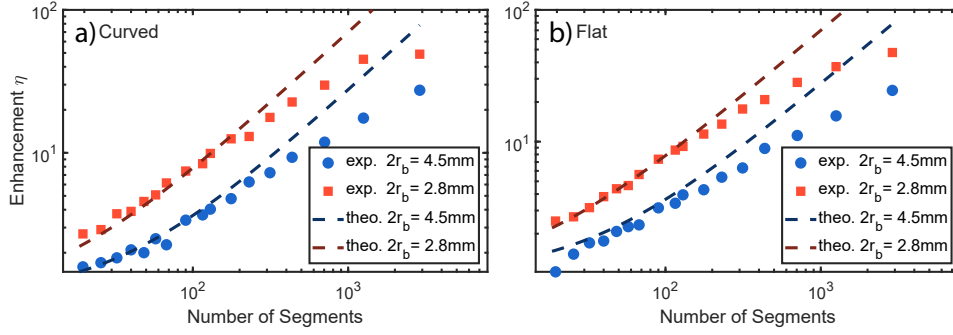
Fig. 6. Enhancement versus the number of active modulating segments for a) flat shape and b) curve shape. On each plot, we show the enhancement for the maximum ($2r_b = 4.5mm$, blue circles) and minimum ($2r_b = 3.8mm$, red squares) illumination radius. The dashed lines show the theoretical enhancement corrected based on r_b.

Although the optimization process does not depend on r_o directly, it depends on r_o: to get the maximum enhancement, the optimization area must have the same size as a single speckle $r_o = r_s$. The size of this single speckle in the detector plane depends on the design of the experiment, particularly if we use or not a lens at the detector. For our measurements, we use a lens-less system, hence the size of a single speckle is in solid angle and equal to [31].

$$r_s = \frac{2.44 \cdot \lambda}{4r_b} d, \tag{4}$$

with λ the wavelength of the incident light and d the thickness of the sample. We infer from Eq 4 that r_o and r_b are inversely related, which means the optimization process depends on both parameters.

In Ref. [32], Ojambati and co-workers studied how the maximum enhancement changes when changing r_o, thus $\eta_0' = \eta_0'(r_o)$. This dependency is expressed as [32]

$$\eta_0'(r_o) = \frac{K}{r_o^2} + 1, \tag{5}$$

where the correction factor K depends on the number of segments N_s and on the speckle size. The theoretical limit η_0 is reached when r_o approaches the speckle size $r_s(r_b)$, $\lim_{r_o \to r_s(r_b)} \eta_0'(r_o) = \eta_0$. If we take the limiting value of $r_o = r_s(r_b)$ in Eq. 5 and we replace it with Eq. 4, and we take the limiting value of $\eta_0'(r_o) = \eta_0$ and we replace it with Eq. 3, we obtain an extended correction factor $K(N_s, r_b)$:

$$K(N_s, r_b) = \frac{2.44^2 \pi \lambda^2}{4^3 r_b^2} d^2 (N_s - 1). \tag{6}$$

Finally, the theoretical enhancement corrected for optimization and beam areas is given by

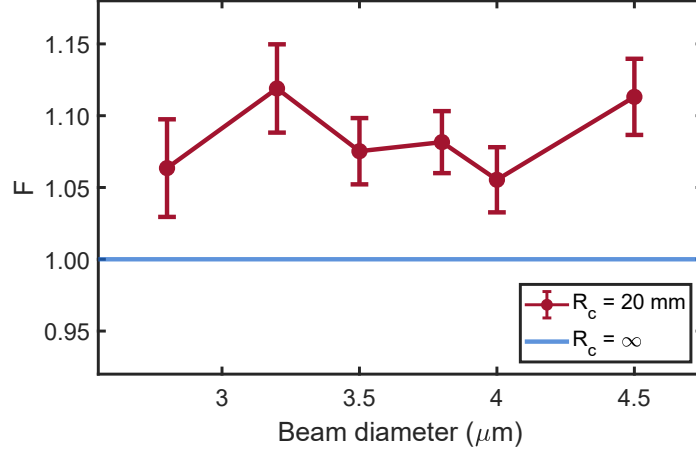$$\eta_0'(r_o, r_b) = \frac{2.44^2 \pi \lambda^2}{4^3 r_b^2 r_o^2} d^2 (N_s - 1) + 1. \tag{7}$$

Fig. 7. The figure of merit (F) versus beam diameter $2r_\mathrm{b}$. The figure of merit is based on comparing a curved sample with $R_\mathrm{c} = 20$ mm and a flat sample ($R_\mathrm{c} = \infty$). The light blue line corresponds to the case when the curvature is not changed, *i.e.*, $FoM = 1$.

In Eq. 7 we see that the enhancement is inversely proportional to r_b^2 and r_o^2, and directly proportional to d^2. Both dependencies are in accordance with usual WFS experiments, where one focuses the incident beam to a narrow spot and reduces the optimization area to a single speckle, while placing the detector far from the sample to increase the size of the speckle on the detector. In our experiments r_o is fixed, and we compare the measurements while varying r_b.

5. Effect of sample curvature

We study the impact of the ratio between the beam radius r_b and the radius of curvature of the sample R_c. We vary the radius r_b in a range between 1.9 mm and 2.3 mm (hence diameters $2r_\mathrm{b} = 3.8$ to 4.6 mm) by changing the position of the focusing lens L5 (see Fig. 2). We measure the enhancement versus number of segments N_s (as in Fig 3) for six different beam radii r_b and both flat and curved sample's shapes.

Fig. 6 shows the enhancements for the lowest and highest r_b for both shapes, along with the maximum theoretical limit for each case, calculated from Eq. 7. We see that the enhancement decreases when increasing the beam radius, and so does the theoretical limit, in accordance with our theory (see Eq. 7). When increasing r_b, the speckle size is smaller. If r_o is constant, there are more speckles inside the optimization area, thus the maximum enhancement is lower.

Finally, we compare the enhancement of a curved and a flat sample for different r_b. For this comparison, we propose the following figure of merit F, defined as:

$$F \equiv \langle \frac{\eta_\mathrm{curve}}{\eta_\mathrm{flat}} \rangle_N, \tag{8}$$

with η_curve the enhancement for the curve shape, η_flat the enhancement for the flat shape, and $\langle . \rangle_N$ the *geometric mean* over the number of segments N. This figure of merit is applicable regardless of the shift shown in Fig. 6 because we expect this shift to occur both in the flat and the curved shape.

We show F in Fig. 7 for different beam radii. We see that F is constant at about $F = 1.08$ and it is independent of r_b.

Finally, we see that all data are larger than $F = 1$, showing that, on average, we achieve a larger enhancement with a curve shape instead of a flat shape. This challenges the current theoretical framework of wavefront shaping because no fundamental scattering property was changed except the macroscopic sample's shape and the position of the lens, yet based on this figure of merit, the enhancement difference is statistically significant.

6. Conclusions

In this paper, we studied how the intensity enhancement obtained using wavefront shaping changes when we change the macroscopic properties of the object. We compare the case of two macroscopic shapes, a free-form curved sample and a flat sample with a slab shape. We used a tailored-made sample holder to change the curvature of a flexible sample and a focusing lens with a linear stage to change the beam radius on the sample.

We see a low correlation between the optimal wavefronts for different macroscopic shapes, suggesting a change in the light transport inside the scattering media at a mesoscopic level. Meanwhile, when optimizing the intensity using the wavefront shaping technique, we reach a similar enhancement for a curved sample as for a flat sample. This performance persistence is in agreement with our hypothesis; regardless of the changes in light transport, the number of open channels is unchanged, thus the maximum enhancement is not affected by these changes. Our results confirm the idea that wavefront shaping is applicable regardless of the form of the object.

We derive an extension of the theory for maximum enhancement based on the beam and optimization radius. Our experiments are in agreement with our theoretical prediction, and our theory explains the trend for both a curved and flat sample. Furthermore, we propose a figure of merit to compare the enhancement between different shapes. Based on this figure of merit, we see an increase in the total enhancement by 10% for every beam radius. This increase is not explained using current theories based on slab shapes only.

With this paper, we aim to encourage the community to consider free-form objects both in experiments and theory of light scattering, as they have a larger impact on industrial applications. The next steps in this project include studying speckle decorrelation in real-time while changing the form of the sample and measuring samples with various densities of scatterers.

Disclosures. The authors declare no conflicts of interest.

Data availability. The data used for this publication are publicly available in the Zenodo database in Ref. [33].

References

1. R. Winston, J. C. Miñano, and P. Benítez, eds., *Nonimaging Optics* (Academic Press, Burlington, 2005).
2. F. Fang, X. Zhang, A. Weckenmann, G. Zhang, and C. Evans, "Manufacturing and measurement of freeform optics," CIRP Ann. **62**, 823–846 (2013).
3. S. Nakamura, "Background story of the invention of efficient blue ingan light emitting diodes (nobel lecture)," Ann. der Physik **527**, 335–349 (2015).
4. E. F. Schubert, *Light-Emitting Diodes* (Cambridge University Press, 2006), 2nd ed.
5. M. R. Krames, O. B. Shchekin, R. Mueller-Mach, G. O. Mueller, L. Zhou, G. Harbers, and M. G. Craford, "Status and future of high-power light-emitting diodes for solid-state lighting," J. Disp. Technol. **3**, 160–175 (2007).
6. I. M. Vellekoop and A. P. Mosk, "Focusing coherent light through opaque strongly scattering media," Opt. Lett. **32**, 2309–2311 (2007).

7. A. P. Mosk, A. Lagendijk, G. Lerosey, and M. Fink, "Controlling waves in space and time for imaging and focusing in complex media," Nat. Photon. **6**, 283—-292 (2012).
8. S. M. Popoff, A. Goetschy, S. F. Liew, A. D. Stone, and H. Cao, "Coherent control of total transmission of light through disordered media," Phys. Rev. Lett. **112**, 133903 (2014).
9. I. M. Vellekoop, "Feedback-based wavefront shaping," Opt. Express **23**, 12189–12206 (2015).
10. S. Rotter and S. Gigan, "Light fields in complex media: Mesoscopic scattering meets wave control," Rev. Mod. Phys. **89**, 015005 (2017).
11. M. Nixon, O. Katz, E. Small, Y. Bromberg, A. A. Friesem, Y. Silberberg, and N. Davidson, "Real-time wavefront shaping through scattering media by all-optical feedback," Nat. Photonics **7**, 919–924 (2013).
12. R. Horstmeyer, H. Ruan, and C. Yang, "Guidestar-assisted wavefront-shaping methods for focusing light into biological tissue," Nat. Photonics **9**, 563–571 (2015).
13. S. Gigan, O. Katz, H. B. de Aguiar, E. R. Andresen, A. Aubry, J. Bertolotti, E. Bossy, D. Bouchet, J. Brake, S. Brasselet, Y. Bromberg, H. Cao, T. Chaigne, Z. Cheng, W. Choi, T. Čižmár, M. Cui, V. R. Curtis, H. Defienne, M. Hofer, R. Horisaki, R. Horstmeyer, N. Ji, A. K. LaViolette, J. Mertz, C. Moser, A. P. Mosk, N. C. Pégard, R. Piestun, S. Popoff, D. B. Phillips, D. Psaltis, B. Rahmani, H. Rigneault, S. Rotter, L. Tian, I. M. Vellekoop, L. Waller, L. Wang, T. Weber, S. Xiao, C. Xu, A. Yamilov, C. Yang, and H. Yılmaz, "Roadmap on wavefront shaping and deep imaging in complex media," J. Physics: Photonics **4**, 042501 (2022).
14. R. Sarma, A. Yamilov, and H. Cao, "Enhancing light transmission through a disordered waveguide with inhomogeneous scattering and loss," Appl. Phys. Lett. **110**, 021103 (2017).
15. R. Uppu, M. Adhikary, C. A. M. Harteveld, and W. L. Vos, "Spatially shaping waves to penetrate deep inside a forbidden gap," Phys. Rev. Lett. **126**, 177402 (2021).
16. I. Freund, M. Rosenbluh, and S. Feng, "Memory effects in propagation of optical waves through disordered media," Phys. Rev. Lett. **61**, 2328–2331 (1988).
17. S. Feng, C. Kane, P. A. Lee, and A. D. Stone, "Correlations and fluctuations of coherent wave transmission through disordered media," Phys. Rev. Lett. **61**, 834–837 (1988).
18. B. Judkewitz, R. Horstmeyer, I. M. Vellekoop, I. N. Papadopoulos, and C. Yang, "Translation correlations in anisotropically scattering media," Nat. Phys. **11**, 684–689 (2015).
19. F. van Beijnum, E. G. van Putten, A. Lagendijk, and A. P. Mosk, "Frequency bandwidth of light focused through turbid media," Opt. Lett. **36**, 373–375 (2011).
20. W.-H. Lee, "III computer-generated holograms: Techniques and applications," in *Progress in Optics,* vol. 16 E. Wolf, ed. (Elsevier, 1978), pp. 119–232.
21. D. B. Conkey, A. M. Caravaca-Aguirre, and R. Piestun, "High-speed scattering medium characterization with application to focusing light through turbid media," Opt. Express **20**, 1733–1740 (2012).
22. I. M. Vellekoop and A. P. Mosk, "Universal optimal transmission of light through disordered materials," Phys. Rev. Lett. **101**, 120601 (2008).
23. J. Aulbach, B. Gjonaj, P. Johnson, and A. Lagendijk, "Spatiotemporal focusing in opaque scattering media by wave front shaping with nonlinear feedback," Opt. Express **20**, 29237–29251 (2012).
24. I. Freund, "Looking through walls and around corners," Phys. A **168**, 49—-65 (1990).
25. M. C. W. van Rossum and T. M. Nieuwenhuizen, "Multiple scattering of classical waves: microscopy, mesoscopy, and diffusion," Rev. Mod. Phys. **71**, 313–371 (1999).
26. F. Pedregosa, G. Varoquaux, A. Gramfort, V. Michel, B. Thirion, O. Grisel, M. Blondel, P. Prettenhofer, R. Weiss, V. Dubourg, J. Vanderplas, A. Passos, D. Cournapeau, M. Brucher, M. Perrot, and E. Duchesnay, "Scikit-learn: Machine learning in Python," J. Mach. Learn. Res. **12**, 2825–2830 (2011).
27. M. Adhikary, "Controlled light propagation in random, periodic, and superperiodic silicon nanophotonic materials," Ph.D. thesis, University of Twente, Netherlands (2021).
28. E. P. Wigner, "On the statistical distribution of the widths and spacings of nuclear resonance levels," Math. Proc. Camb. Philos. Soc. **47**, 790–798 (1951).
29. T. Guhr, A. Müller–Groeling, and H. A. Weidenmüller, "Random-matrix theories in quantum physics: common concepts," Phys. Reports **299**, 189–425 (1998).
30. K. L. van der Molen, R. W. Tjerkstra, A. P. Mosk, and A. Lagendijk, "Spatial extent of random laser modes," Phys. Rev. Lett. **98**, 143901 (2007).
31. E. Fujiwara, J. A. Fracarolli, and C. M. B. Cordeiro, "Didactic laser speckle experiments with a lensless camera," Eur. J. Phys. **42**, 065303 (2021).
32. O. S. Ojambati, J. T. Hosmer-Quint, K.-J. Gorter, A. P. Mosk, and W. L. Vos, "Controlling the intensity of light in large areas at the interfaces of a scattering medium," Phys. Rev. A **94**, 043834 (2016).
33. A. Rates, "Wavefront shaping through a free-form scattering object," .